

## Article

# Analysis of the Temperature Field Effect on the Thermal Stress of the Main Tower of Long-Span Suspension Bridges

Maojun Duan , Juntian Zhu, Zhong Gu, Zijun Fang and Jiaying Xu

College of Civil Engineering, Nanjing Forestry University, Nanjing 210037, China; zjt814422722@163.com (J.Z.); gz19805165917@163.com (Z.G.); 18130438993@163.com (Z.F.); 18879106142@163.com (J.X.)

\* Correspondence: dmj@njfu.edu.cn

**Abstract:** To investigate the temperature field variation of the main tower of large-span suspension bridges, the Nanjing Xinchengwei Yangtze River Bridge was selected as the objective of the present study. The finite element model of the main tower was developed, and the analysis of the effect of the temperature field on the structure of the main tower was carried out. The calculation parameters of the temperature field of the main tower were determined, and the influence of the solar radiation temperature of the main tower within 24 h was investigated. Differences in the temperatures inside and outside the wall of the tower column were analyzed, and the thermal stress of the tower wall under the most unfavorable temperature difference was calculated. Results show that under the positive temperature difference, the area of tensile stress is mainly concentrated on the inner wall, the maximum value is located at the corner of the intersection of the tower wall, and the range of tensile stress is mainly diffused along the vertical wall. Under the action of negative temperature difference, the area of tensile stress is mainly concentrated in the outer tower wall, the maximum value is located in the upper part of the western outer tower wall, and the range of tensile stress is mainly diffused along the center of the tower wall to both sides. The maximum tensile stresses in the inner and outer tower wall are 2.8 MPa and 1.3 MPa, respectively, which meets the standard value of 2.85 MPa for the tensile strength of C60 concrete specified in the Chinese national standard.

**Keywords:** temperature field; main tower; thermal stress; finite element analysis



**Citation:** Duan, M.; Zhu, J.; Gu, Z.; Fang, Z.; Xu, J. Analysis of the Temperature Field Effect on the Thermal Stress of the Main Tower of Long-Span Suspension Bridges. *Appl. Sci.* **2023**, *13*, 8787. <https://doi.org/10.3390/app13158787>

Academic Editors: Wenming Zhang, Xiaoming Wang, Yuan Sun and Hongyou Cao

Received: 21 June 2023  
Revised: 24 July 2023  
Accepted: 26 July 2023  
Published: 29 July 2023



**Copyright:** © 2023 by the authors. Licensee MDPI, Basel, Switzerland. This article is an open access article distributed under the terms and conditions of the Creative Commons Attribution (CC BY) license (<https://creativecommons.org/licenses/by/4.0/>).

## 1. Introduction

The concrete tower is an important component of cable-stayed bridges, suspension bridges, and other structural systems. Cracks in thin-walled structures (e.g., the main concrete tower) during the service period have become a new problem for mass concrete structures [1,2]. In particular, the solar radiation temperature variation will cause the temperature difference between the inner and outer walls of the tower column, forming a certain temperature difference stress, which often exceeds the stress generated by the structure's dead load, live load, and other loads, and usually leads to excessive local stress and crack failure [3–5].

At present, the research on the temperature effect of concrete bridge structures mainly focuses on the upper concrete box girder structure, while the temperature field effect of the lower structure is rarely studied, such as the prestressed concrete continuous rigid frame bridge, cable-stayed bridge, concrete piers and tower columns of suspension bridges [6]. Zhu et al. [7] proposed a numerical simulation analysis method for the temperature field and stress field of concrete through real-time monitoring of the instantaneous temperature field and strength field of the internal temperature of concrete. Li et al. [8] proposed the solar temperature field model of the main tower of the cross-sea cable-stayed bridge through transient heat transfer analysis. By introducing major parameters such as solar elevation angle, azimuth angle, and radiation absorption coefficient, the accuracy of the proposed model was verified by comparing the measured data of the temperature field

with predicted values. Wang et al. [9] investigated the influence of solar temperature difference on the deviation and stress of the cable tower under the condition of onsite monitoring of the construction process of the Tieluoping super-large bridge. Feng et al. [10] investigated the thermal stress of the bridge tower, indicating that the generation of vertical cracks in the bridge tower was closely related to the temperature field inside the concrete tower. In addition, concrete cracks would close and re-open under the action of different temperature fields. Huang et al. [11] reduced the size of a concrete arch bridge by five times, and the calculated temperature isoline and temperature time-history curve were in good agreement with the measured values, which verified the accuracy of the finite element model. Subsequently, the verified finite element model was used for parameter analysis. The influence of thermal parameters on thermal behavior was discussed, and an effective thermal control method was proposed. Jin et al. [12] took a cable-stayed bridge with a steel box girder as an example to discuss the influence of temperature on the beam deflection at different time scales. Results show that the temperature difference of the beam, as well as the temperature gradient, will lead to a large deflection. In general, it could be concluded from the abovementioned investigations that the characteristics of the thermal stress of the main tower induced by the temperature variation differ from each other, mainly depending on the appearance and geometry. However, few studies are focused on the effect of the temperature field on the thermal stress of the unique gate-shaped steel-concrete composite main tower of the Nanjing Xinchengwei Yangtze River Bridge (i.e., the engineering background of the present study), which is with a main span of 1760 m. Therefore, it is necessary to comprehensively investigate the characteristics of the thermal stress of the main tower of the Nanjing Xinchengwei Yangtze River Bridge.

In this paper, by selecting the Nanjing Xinchengwei Yangtze River Bridge as the engineering background, the analysis of the effect of the temperature field on the thermal stress of the main tower structure was carried out to investigate the effect of the solar temperature field within 24 h. The difference in the temperature between the inner and outer walls of the tower and its variation trend were analyzed. The temperature difference stress of the tower wall under the most unfavorable temperature difference was calculated, and the variation trend of the stress and deflection of each column segment caused by the overall rising and cooling was also calculated. Conclusions could provide a significant reference value for the construction and operation of the main tower of similar bridge structures.

## 2. Engineering Background

Nanjing Xinchengwei Yangtze River Bridge is a double-tower steel box girder suspension bridge with a span of 580 m + 1760 m + 580 m. The ratio of main span to main cable span is 1/9, ranking the first in China and the second in the world among similar bridges. The stiffening beam is closed with a flat and streamlined integral steel box girder. The main cable adopts a prefabricated parallel high-strength steel wire strand structure (PPWS). Each main cable is composed of 169 strands, and each share is composed of 127 galvanized aluminum alloy high-strength steel wires with a diameter of 5.4 mm. The elevation layout and in-site construction images are given in Figures 1 and 2.

The main tower is a double-limb door-shaped reinforced concrete tower with a full height of 263.8 m, which is composed of upper, middle and lower columns, upper and lower beams, and top saddle. The transverse center spacing between the two columns is 27.7 m at the top of the tower and 42.7 m at the bottom of the tower. Its structure diagram and onsite construction images are given in Figures 3 and 4.

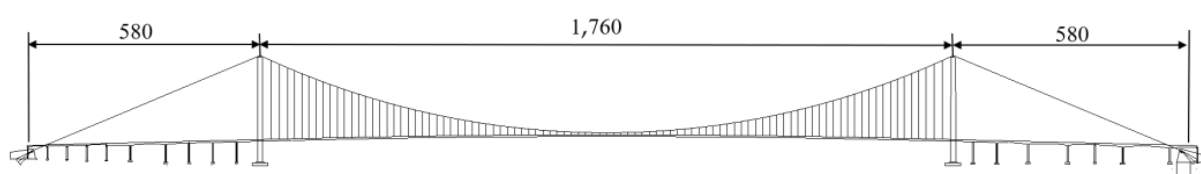


**Figure 1.** Elevation layout of main bridge of Nanjing Xinchengwei Yangtze River Bridge (Unit: m).



Figure 2. Construction site of Nanjing Xinshengwei Yangtze River Bridge (Images taken by Maojun Duan).

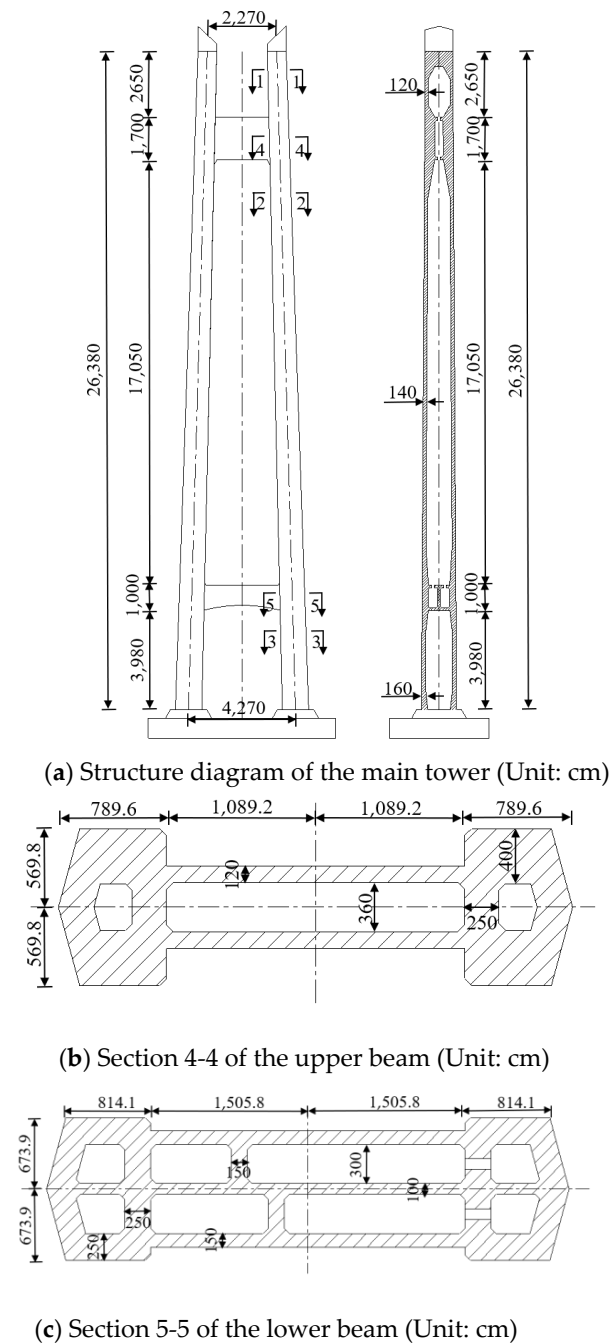


Figure 3. Structure diagram of the main tower.



(a) The main tower



(b) Construction site of the upper beam



(c) Construction site of the lower beam

**Figure 4.** Onsite construction image of the main tower.

### 3. Finite Element Modeling of the Main Tower

#### 3.1. Development of the Solid Model

A finite element (FE) model simulating the main tower of Nanjing Xinchengwei Yangtze River Bridge was developed by using MIDAS FEA v4.0, as shown in Figure 5, where X, Y, and Z direction is horizontal, longitudinal and vertical, respectively. In this

model, the chamfered part of the contact area between the main tower column and the upper and lower beams, the prestressed steel bars in the beams, and the constraints between the temporary transverse struts and the concrete tower columns are considered in detail. However, in the modeling process, the influence of ordinary structural steel bars is not taken into account for the convenience of calculation. To develop the FE model, 3D solid units were adopted to simulate the concrete column, as well as the upper and lower beams. Meanwhile, 1D line units were adopted to simulate the temporary cross braces and prestressed steel bundles.

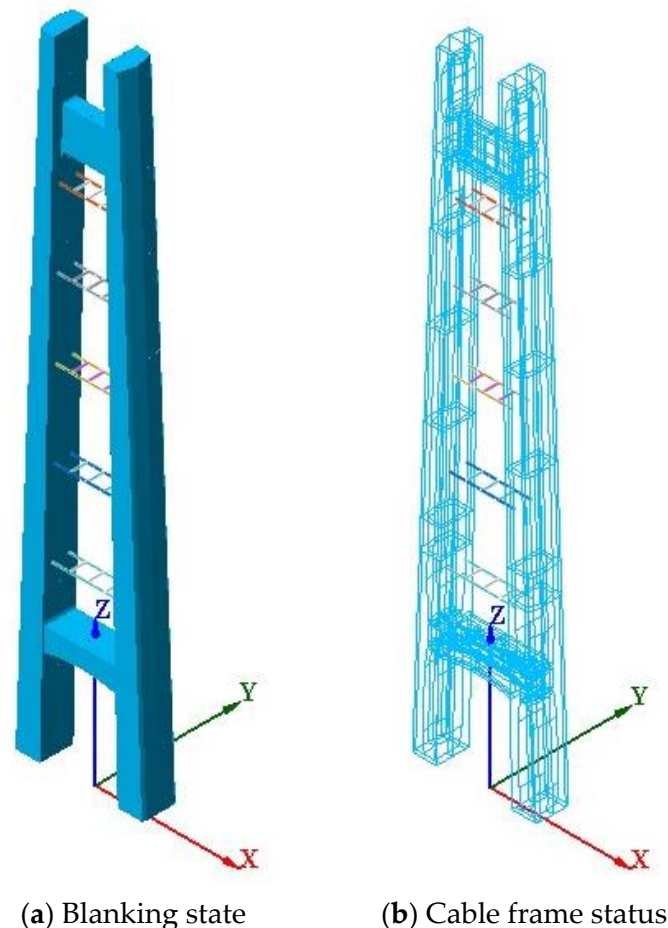


**Figure 5.** Finite element model of the main tower.

### 3.2. Meshing of the FE Model

In this model, the concrete entity of the main tower is meshed by 4-node and 4-dihedral primary units. Meanwhile, since the main tower is composed of different components and there are many chamfers in the contact area between the beam and the tower column, the meshed entity technology is adopted by segmenting cutting. To avoid the phenomenon of non-automatic coupling of contact node elements in the grid division of entities with different sections, it is necessary to use the entity difference set operation of Boolean operation in advance for mutual printing of contact surfaces. The meshing size is a key parameter in finite element modeling. For determining the meshing size to be adopted in the present study, mesh sensitivity analysis was conducted by employing the meshing size of 1.0 m, 0.5 m and 0.2 m, respectively. The thermal stresses on the outer surface of east tower wall at 3:00, 6:00, 9:00, 12:00, 15:00 and 18:00 were extracted, as listed in Table 1. It can be seen from Table 1 that the results corresponding to a meshing size of 1.0 m, 0.5 m and 0.2 m show minor difference. Therefore, for improving the computing efficiency, a meshing size of 1.0 m was adopted in the present study.

**Table 1.** Thermal stresses corresponding to different meshing sizes (MPa).

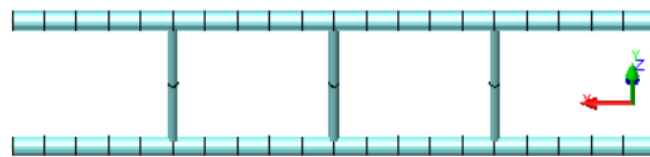
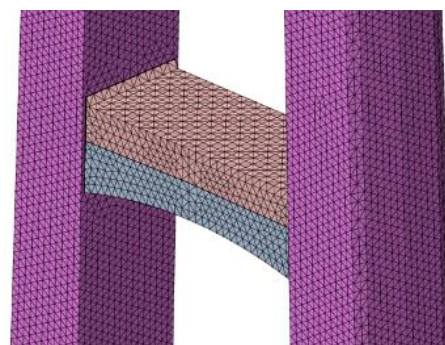
Time Size	3:00	6:00	9:00	12:00	15:00	18:00
1.0 m	0.48076	−0.18956	−1.40343	−2.39181	−2.48554	−1.5524
0.5 m	0.47976	−0.19056	−1.40443	−2.39281	−2.48654	−1.5534
0.2 m	0.47966	−0.19066	−1.40453	−2.39291	−2.48664	−1.5535

The size of the solid grid units on both sides of the tower columns, as well as on the upper and lower beams, is set to be 1 m. In general, there are 266,500 concrete 3D units.

Since the transverse prestressed steel bundle is arranged in a curved direction, the B-spline curve is generated by using the function of “defining line”, and the reinforcement in the solid unit is selected at the same time. The common node combined with embedded constraint and adaptive comparison line grid division method is used to ensure the common force between reinforcement and concrete in the model calculation. The generated prestressed steel beam grid elements are all one-dimensional low-order line elements (regardless of the influence of curvature on friction), and the number is 88,868, as shown in Figure 6. The temporary cross bracing is built with one-dimensional, two-node beam elements. For adaptive grid division, there are 230 beam elements and 45 rigid connection elements at both ends of the temporary cross-bracing, as shown in Figure 7. The grid division diagram of the tower column and the lower beam is shown in Figure 8. There are 157,950 nodes and 355,643 units in the full tower multi-scale model. The conduction differential equation governing the calculation of finite element model could be expressed by Equation (1) [13]:

$$\lambda \left( \frac{\partial^2 T}{\partial x^2} + \frac{\partial^2 T}{\partial y^2} + \frac{\partial^2 T}{\partial z^2} \right) = \rho c \frac{\partial T}{\partial t} \quad (1)$$

where  $\lambda$  is the coefficient of thermal conductivity;  $c$  is the specific heat;  $\rho$  is the density;  $T$  is the temperature; and  $t$  is time.

**Figure 6.** Schematic diagram of prestressed steel bundle.**Figure 7.** Schematic diagram of temporary cross brace division.**Figure 8.** Schematic diagram of column and beam division.

As the thin-walled concrete tower is constrained, the thermal stress will be generated due to the influence of temperature change. The equilibrium equation to determine the thermal stress could be determined by Equation (2) [13]:

$$\begin{cases} \varepsilon_x = \frac{1}{E} [\sigma_x - \nu(\sigma_y + \sigma_z)] + \alpha\Delta T \\ \varepsilon_y = \frac{1}{E} [\sigma_y - \nu(\sigma_x + \sigma_z)] + \alpha\Delta T \\ \varepsilon_z = \frac{1}{E} [\sigma_z - \nu(\sigma_x + \sigma_y)] + \alpha\Delta T \end{cases} \quad (2)$$

where  $\sigma_x$ ,  $\sigma_y$ , and  $\sigma_z$  is the stress component along  $x$ ,  $y$ , and  $z$ -axis, respectively;  $\varepsilon_x$ ,  $\varepsilon_y$ , and  $\varepsilon_z$  is the corresponding strain component;  $E$  is the elastic modulus;  $\nu$  is the Poisson's ratio;  $\alpha$  is the coefficient of thermal expansion; and  $\Delta T$  is the temperature change.

### 3.3. Boundary Conditions

In the modeling process of the main tower, the constraint conditions can be divided into two categories: (1) constraints corresponding to the main tower; and (2) external construction constraints. External construction constraints refer to the contact between the prestressed steel bundle in the upper and lower beams of the main tower and the concrete entity, as well as the connection constraints between the two ends of the temporary transverse braces and the two sides of the tower wall during construction [14]. The types of constraints are summarized in Table 2. As listed in Table 1, the nodes at the bottom of the main tower were constrained, i.e., the displacements and rotation along X-, Y- and Z-axis were set to be zero. The prestressed steel bundles and concrete were embedded together, i.e., the elements in the model of the steel bundle and concrete shared the same node at the interface. In terms of the boundary conditions of the temporary cross braces, the nodes at the interface between the temporary cross braces and the tower columns were fixed, i.e., different elements adopted the same node at the interface. The diagram of the physical boundary conditions was plotted in Figure 9. In terms of the heat conducting boundary conditions, the governing equation could be expressed by Equation (3) [13]:

$$\lambda \frac{\partial T}{\partial n} + (h_c + h_r)(T - T_a) = 0 \quad (3)$$

where  $n$  is the normal direction of the boundary surface;  $h_c$  is the convective heat transfer coefficient;  $h_r$  is the radiation heat transfer coefficient; and  $T_a$  is the temperature of the air around the outer interface.

The governing equation for determining the thermal stress could be expressed by Equation (4) [13]:

$$\begin{cases} \sigma_x l + \tau_{xy} m + \tau_{xz} n = 0 \\ \sigma_y m + \tau_{yx} l + \tau_{yz} n = 0 \\ \sigma_z n + \tau_{zx} l + \tau_{zy} m = 0 \end{cases} \quad (4)$$

where  $\tau_{xy}$ ,  $\tau_{xz}$ ,  $\tau_{yx}$ ,  $\tau_{yz}$ ,  $\tau_{zx}$  and  $\tau_{zy}$  are the stress component;  $l$ ,  $m$  and  $n$  are the component of the surface unit normal vector in all directions.

**Table 2.** Constraints of the finite element model.

Constraint Object	Constraint Type
Bottom of the main tower	All nodes and units are constrained
Prestressed steel beam with concrete	embedment
Temporary cross braces and tower walls	Multi-point rigid connection

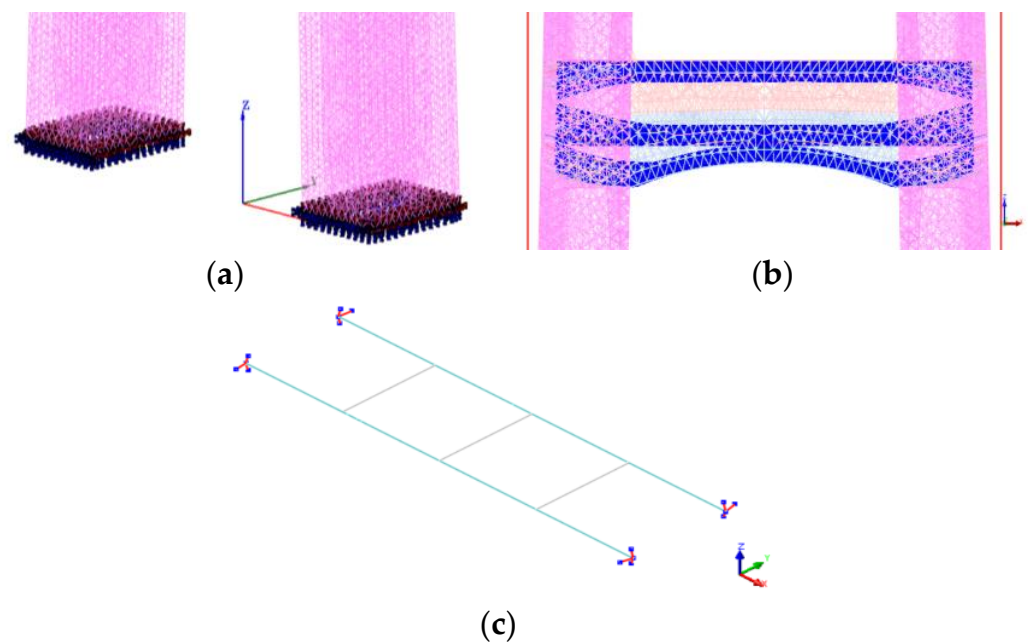


**Figure 9.** Constraints of the main tower. (a) Constraints at the bottom of the main tower. (b) Prestressed steel bundles and concrete constraints. (c) Temporary transverse brace at both ends of the constraint.

#### 4. Determination of the Calculation Parameters of the Temperature Field

##### 4.1. Environmental Parameters of the Main Tower

In the simulation analysis of the temperature field effect of the main tower, the environmental parameters to be determined mainly include the geographical location of the main tower and the surrounding air temperature, which is the advanced condition to analyze the temperature distribution and heat conduction characteristics of the main tower. According to the investigation, the main tower of Nanjing Xinshengwei Yangtze River Bridge is located in Qixia District in Nanjing City. The geographical latitude is  $32.14^\circ$  north latitude and  $118.89^\circ$  east longitude. The climate belongs to the subtropical monsoon humid climate zone, and the annual average temperature is  $15.14^\circ\text{C}$  throughout the year. In this paper, the average annual temperature of Nanjing is valued at  $15.14^\circ\text{C}$  to determine the air temperature around the main tower.

##### 4.2. Atmosphere and Solar Radiation Temperature Parameters around the Main Tower

The atmospheric temperature changes with the solar radiation temperature, which mainly affects the convective heat transfer when the inner and outer walls of the main tower contact with the air, resulting in different humidity distribution on the section of the main tower [15]. The greater the daily variation of atmospheric temperature and humidity around the main tower, the greater the temperature difference between the inner and outer walls of the column section. In the process of analyzing the temperature field of the main tower, the time node interpolation method and the sine function are mainly used for numerical simulation to determine the temperature field distribution of the tower wall. Many scholars have found through investigation that there is an obvious diurnal variation law of atmospheric temperature and solar radiation temperature in China, that is, the temperature is lowest between 6 a.m. and 8 a.m., then gradually rises, reaches the highest point between 12 a.m. and 3 p.m., and then gradually drops. The variation law is similar to a sine function. Therefore, the sine function is used in this paper to describe the

diurnal variation of atmosphere and solar radiation temperature around the main tower, as expressed by Equation (5) [13]:

$$F(t) = T \sin \frac{\pi}{12(t + t_0)} + T_0 \tag{5}$$

where  $T$  for air and solar radiation temperature range ( $^{\circ}\text{C}$ );  $T_0$  for air and sunshine average temperature ( $^{\circ}\text{C}$ );  $t_0$  for maximum and minimum air and solar radiation temperature time delay.

As the main tower box room will not be affected by sunlight and almost no air convection exists, the temperature is relatively stable. Therefore, the indoor temperature of the main tower chamber was taken as the daily average atmospheric temperature for simulation.

#### 4.3. Thermal Parameters of Concrete

In the analysis of the temperature field effect of the main tower, the basic thermal parameters of concrete should be determined first. The main tower of Nanjing Xinchengwei Yangtze River Bridge is cast and formed by concrete typed C60 in the whole process. The values of weight density, elastic modulus, Poisson’s ratio, coefficient of thermal expansion, heat conductivity, specific heat capacity, and heat source coefficient [13] are shown in Table 3.

**Table 3.** Basic thermal parameters of the concrete typed C60 [13].

Weight Density (kN/m <sup>3</sup> )	Modulus of Elasticity (MPa)	Poisson’s Ratio	Coefficient of Thermal Expansion (1/ $^{\circ}\text{C}$ )	Thermal Conductivity (W/m)	Specific Heat Capacity (J/kg. $^{\circ}\text{C}$ )	Heat Source Coefficient
26	$3.60 \times 10^4$	0.2	$1 \times 10^{-5}$	2.7	1176	1

#### 4.4. Convection Heat Transfer Parameters

The convective heat transfer between the main tower surface and the air is a complicated heat conduction phenomenon. The efficiency of convective heat transfer depends on many factors, such as ambient air temperature, wind speed, humidity, etc., so the relationship between them is usually determined through tests or empirical formulas [16]. In this way, the heat transfer between the surface of the main tower and the air can be more accurately calculated to analyze and predict the temperature field effect and heat conduction characteristics of the main tower [17]. Among the many influencing factors, wind speed is the most dominant influencing factor. As the wind speed (direction) is constantly changing, the higher the wind speed level is, the higher the heat transfer efficiency will be. Therefore, wind speed is generally used to determine the coefficient of convective heat transfer in the simulation calculation of the temperature field [18]. However, unified value corresponding to the convective heat transfer coefficient is inaccessible. Different values might be employed by different scholars, e.g., the values adopted by Zhang et al. [13], Dai et al. [19], Zhang et al. [20] and Larsson et al. [21] are listed in Table 4.

**Table 4.** Convective heat transfer coefficient selected by scholars at home and abroad (W/m<sup>2</sup>. $^{\circ}\text{C}$ ).

Position Name	Roof Surface	The Outer Surface of the Web	The Bottom Surface	The Inner Surface of the Box Girder
Zhang et al. [13]	14.30	13.30	12.34	9.30
Dai et al. [19]	15.23	/	15.14	10.20
Zhang et al. [18]	11.60	9.60	7.60	5.60
Larsson et al. [20]	11.40	9.50	7.60	5.70

Based on the basic values provided in Table 3, the convection heat transfer coefficients on the outer surface of the main tower were all 13 W/m<sup>2</sup>. $^{\circ}\text{C}$  for simulation in the tempera-

ture field effect analysis of the main tower. It is noted that, as the Nanjing Xinhengwei Yangtze River Bridge is under construction and installing sensors in the tower wall is not permitted, monitoring data for validating the finite element model is unavailable. However, the modelling method adopted in the present study is the same as the one adopted by Ren et al. [22], in which the numerical results are compared to the test data of the solar radiation temperature field of the thin-walled concrete tower. Therefore, it is believed that the modelling method employed in the present study is feasible and the numerical results are acceptable.

### 5. Layout of Points for the Extraction of Temperature

The basic trend of the Nanjing Xinhengwei Yangtze River Bridge is north-south. When the sun shines directly on the east side of the main tower at sunrise in the morning, the temperature of the outer tower wall on the east side is higher than that on the west side of the main tower. With the change of time, the sun moves to the west side of the main tower in the afternoon, and the east side of the main tower is in a shadow area. The temperature of the outer tower wall on the west side increases while the temperature on the east side decreases. Under the influence of the temperature of the solar radiation, the main tower will produce a temperature field gradient, thus causing temperature deformation.

Therefore, to determine the variation of the temperature field of the tower column under the most unfavorable high-temperature weather, the temperature difference between the two sides of the main tower caused by sunshine on one day on 14 August 2022, will be simulated. The structural detail around the 12th column is complex, as the chamfer, transverse partition, hole and prestressed steel bundle exist in the connecting part between the beam and column of the main tower [23]. It is believed that the temperature field corresponding to the selected 12th column is more sensitive to the solar radiation. If the 12th column can maintain good structural performance under the most unfavorable temperature, the whole bridge tower is believed to be within the safe range. Therefore, the 12th column was selected in the present study. The east, south and west tower walls are alternately replaced as the sunshine area, while the north tower walls are always the shadow area, and three temperature measuring points are set on the inner and outer walls. The layout of points (i.e., A1-A3, B1-B3, C1-C3) for the extraction of temperature is shown in Figure 10.

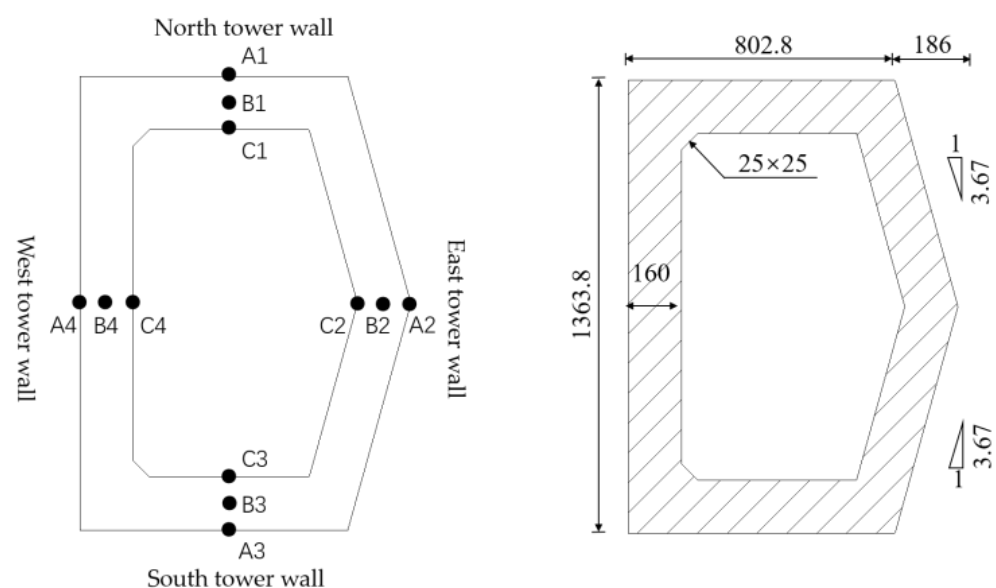


**Figure 10.** The layout of points for the extraction of temperature (unit: cm).

## 6. Stress Analysis of the Bare Tower Subjected to Solar Radiation Variation

### 6.1. Temperature Field Heat Conduction Theory

The heat exchange of the main concrete tower is mainly energy transfer, which is manifested as the temperature change of the inner and outer walls of the tower column. There are three forms of energy transfer: heat conduction, convection heat transfer, and heat radiation, which have different characteristics.

1. Heat conduction refers to the heat transfer process between the same substance under the action of different temperatures. According to Fourier law, the formula of heat conduction can be expressed by Equation (6) [17]:

$$Q = -\lambda \frac{\varphi T}{\varphi X} \quad (6)$$

On the type of  $Q$  for heat flow density ( $\text{W}/\text{m}^2$ );  $\lambda$  for the coefficient of thermal conductivity ( $\text{W}/\text{m}^2 \text{ } ^\circ\text{C}$ );  $\frac{\varphi T}{\varphi X}$  for heat transfer in the direction of the temperature gradient.

2. Convection heat transfer refers to the energy transfer caused by the temperature difference between the solid surface and the fluid, which can be generally divided into natural convection and forced convection. During the construction and operation of the concrete main tower, a convective heat transfer process is usually generated. That is, energy exchange occurs when the fluid contacts with the tower wall. When the fluid temperature is high, there is also heat conduction effect on the column, and heat transfer efficiency will be reduced under the influence of wind speed. Therefore, the convective heat transfer process is usually described by Newton's cooling equation, as expressed by Equation (7) [13]:

$$Q = K(T_\alpha - T_\beta) \quad (7)$$

On the type of  $T_\alpha$  for pillar surface temperature ( $^\circ\text{C}$ );  $T_\beta$  for pillar surrounding fluid temperature ( $^\circ\text{C}$ );  $K$  for convective heat transfer coefficient ( $\text{W}/\text{m}^2 \text{ } ^\circ\text{C}$ ).

3. Thermal radiation refers to the electromagnetic energy radiated by the object itself interacting with other objects, resulting in the process of energy transfer and heat conversion. When the temperature of the main tower is above absolute zero, it emits thermal radiation, which can be transmitted through vacuum and other media. To calculate the net heat transfer between objects in the thermal radiation process of the main tower, the Stefan–Boltzmann equation is generally adopted, as expressed by Equation (8) [13]:

$$Q = \alpha \eta_0 M_i F_{ij} (T_i^4 - T_j^4) \quad (8)$$

On the type of  $M_i$  for pillar  $i$  through an area ( $\text{m}^2$ );  $T_i$  for pillar  $i$  through absolute temperature ( $^\circ\text{C}$ );  $T_j$  for pillar  $j$  through absolute temperature ( $^\circ\text{C}$ );  $F_{ij}$  pillar  $i$  through to the  $j$  shape factor;  $\eta_0$  to take Stephen–Boltzman constant, take  $5.67 \times 10^{-8} \text{ } ^\circ\text{C}, \text{W}/\text{m}^2$ ;  $\alpha$  for pillar radiation ratio.

### 6.2. Analysis of Temperature Change at Each Time

The variation values of three temperature measuring points on the inner and outer walls of 12 columns within a day were extracted, and the variation trend is shown in Figure 11. As can be seen, the temperature of the outer wall of the four sides of the tower in the daytime is greater than that of the inner wall, forming a positive temperature difference. The main reason is that the heat accumulates in the outer wall of the tower due to the increase of solar radiation and atmospheric temperature in the daytime, while the heat conduction rate of concrete is slow, and the temperature cannot be transferred to the inside immediately. During the night, the solar radiation disappears, and the atmospheric

temperature drops rapidly, so the temperature of the outer tower wall drops. Moreover, after the heat transfer effect of concrete from outside to inside for a long time during the day, the temperature of the inner wall will gradually be higher than that of the outer wall, forming a negative temperature difference. During the whole day, the maximum positive temperature difference of the east, south, and west tower walls is 18.6 °C, 18.1 °C and 19.1 °C at 14:00, 16:00 and 18:00, while the maximum negative temperature difference of the east and west tower walls is 2.1 °C and 4.7 °C at 3:00 and 7:00, respectively. Since the north tower wall has not been directly exposed to the sun, the main source of its heat is the heat transfer of the east and west tower walls, so the temperature fluctuation range of the inner and outer walls is small, the maximum is 0.2 °C, and there is no temperature difference along the wall thickness.

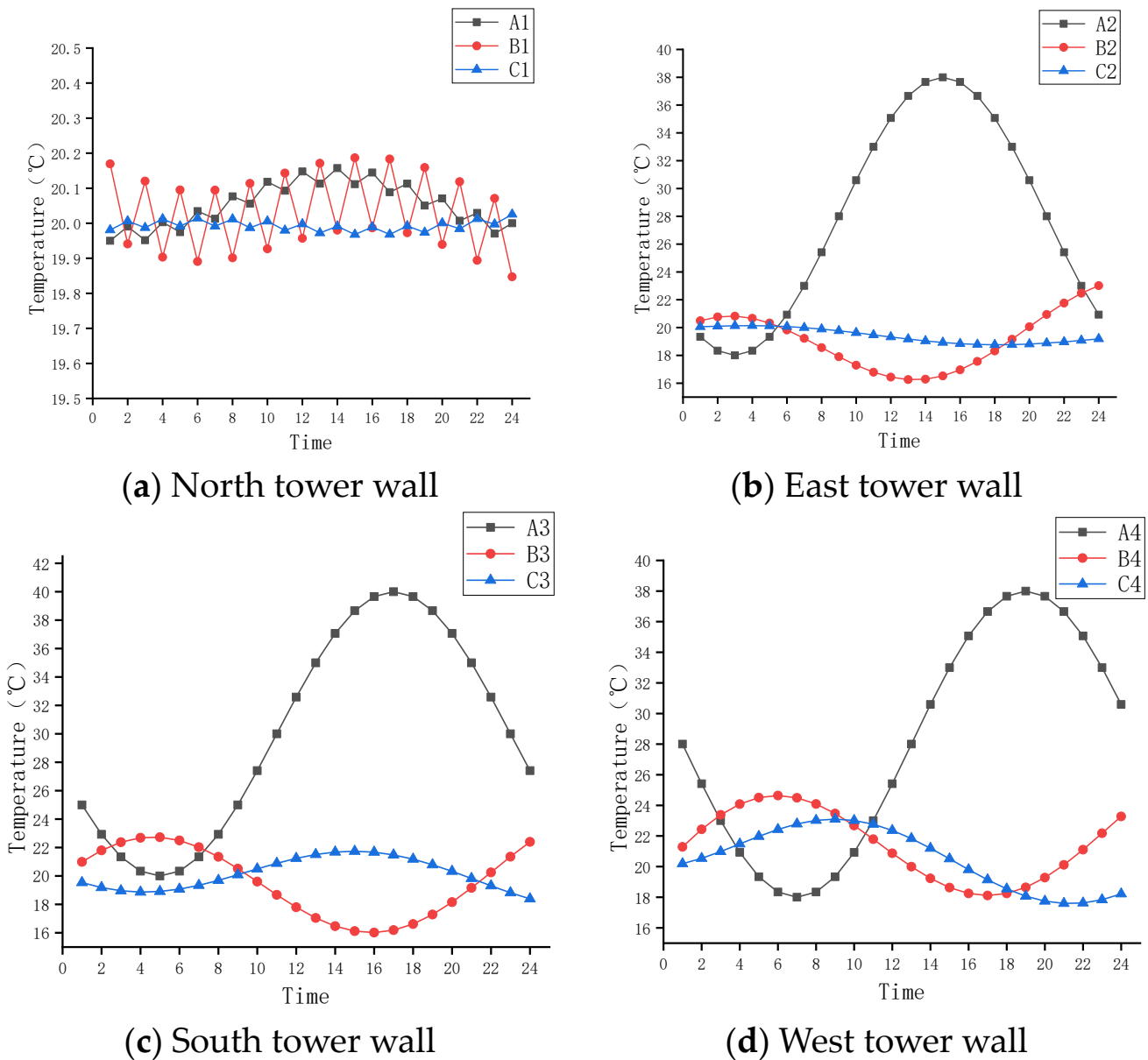


Figure 11. Temperature variation of each side wall of the tower column at any time.

Therefore, to ensure that the main tower will not be damaged by high temperatures in future operation and use, cooling measures can be set at the tower wall in the summer sunshine area, with the focus on the south outer tower wall. The inner wall is not equipped

with cooling facilities because the temperature difference is small, and the temperature is consistent with the ambient temperature.

### 6.3. Analysis of Stress Variation in Temperature Difference at All Times

There are generally two methods for finite element simulation software to calculate thermal stress in the model, that is, the direct coupling method. To save the calculation time of the model, the indirect coupling method is mainly adopted to simulate the change in the thermal stress of the main tower. The specific process is as follows:

1. The general heat transfer conductance analysis of the main tower model is carried out to obtain the temperature results of the node element at the required position at each moment;
2. In the construction phase analysis, the heat conduction result is determined as the thermal load;
3. Extract the corresponding node temperature value as a specific load to apply the forced temperature boundary conditions;
4. Simultaneously calculate the heat conduction analysis and construction phase analysis, and check the required temperature difference stress in the post-processing window.

Through calculation, the temperature difference stress of measuring points on each side of the outer wall and inner wall of the 12th column changes from time to time and are plotted in Figures 12 and 13, where tensile stress is positive and compressive stress is negative. As can be seen, during the solar sunshine period from 6:00 to 18:00 in the daytime, the thermal stress decreases gradually with the increase of the temperature of the outer tower wall, while during the night, the thermal stress increases with the decrease of temperature, and the maximum tensile stress is 1.3 MPa at about 23:00. The thermal stress trend of the inner tower wall is opposite to that of the outer tower wall. During the period from 6:00 to 18:00 when the temperature of the inner tower wall is lower than that of the outer tower wall, the thermal stress keeps increasing, and the maximum tensile stress of the western inner tower wall is 2.7 MPa at 18:00. This phenomenon indicates that the maximum tensile stress occurs in the inner part of the tower wall under the action of positive temperature difference. Under the action of negative temperature difference, the maximum tensile stress will be generated outside the tower wall.

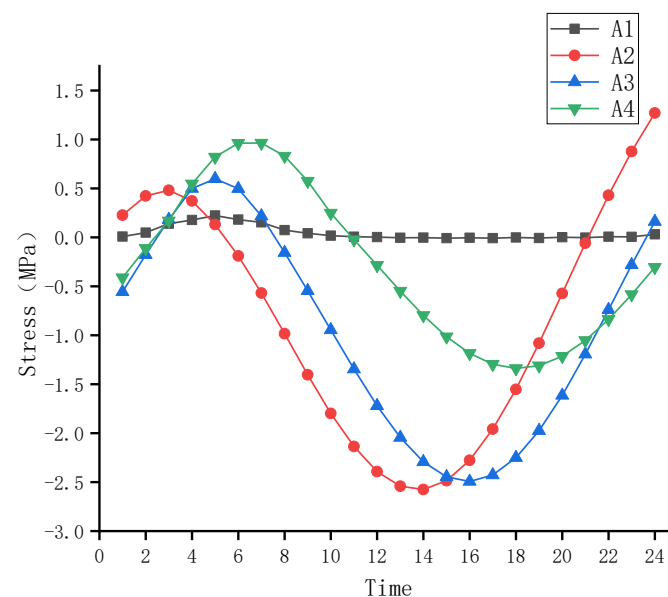


**Figure 12.** Time variation of temperature difference stress at measuring points on the outer wall.

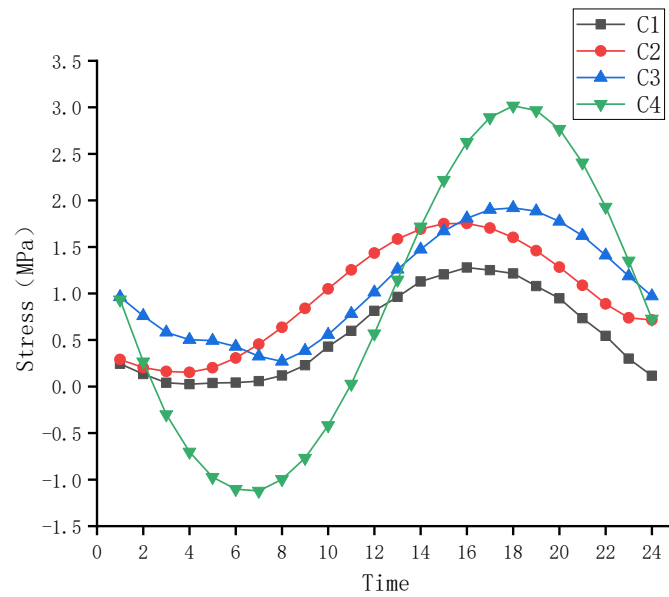


Figure 13. Time variation of temperature difference stress at measuring points on the inner wall.

Figures 14 and 15 show the temperature stress nephogram of the maximum positive temperature difference at 14:00, 16:00 and 18:00 and the maximum negative temperature difference at 3:00 and 7:00. Therefore, in further investigation regarding the in-situ monitoring of temperature variation, monitoring data recorded at 3:00, 7:00, 14:00 and 18:00 must be noticed.

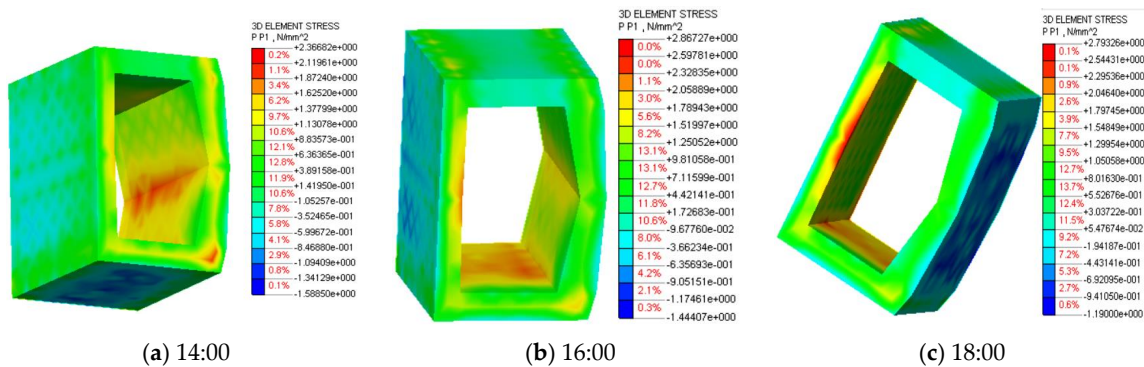


Figure 14. Temperature stress nephogram of maximum positive temperature difference.

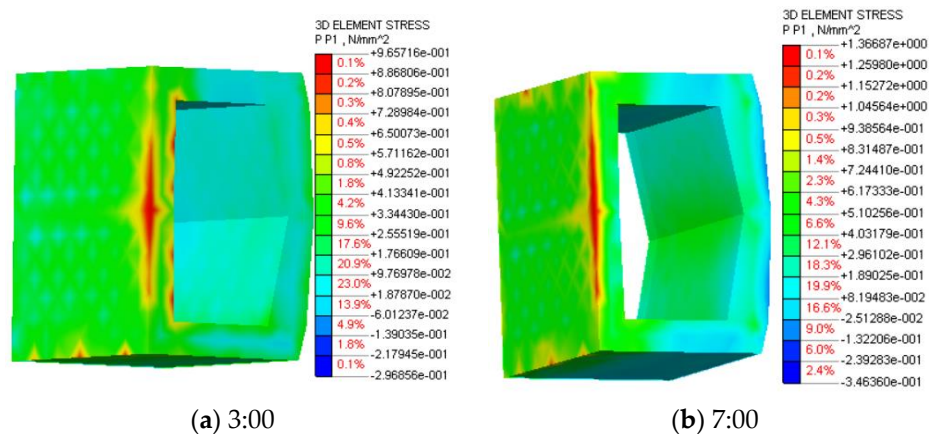


Figure 15. Temperature stress nephogram of maximum negative temperature difference.

As can be seen from Figure 14, under the action of positive temperature difference on the tower wall, the area of tensile stress is mainly concentrated on the inner tower wall; the maximum value is located at the corner where the tower wall intersects, and the range of tensile stress is mainly diffused vertically along the tower wall. The reason could be attributed to the principle of heat expansion and cold contraction: the temperature of the outer wall increases due to solar radiation, hence heat expansion is supposed to happen; however, the outer wall is constrained by the inner wall of which the temperature is less changed, which leads to the compressive stress in the outer wall and tensile stress in the inner wall (see Figure 14). At 14:00, 16:00, and 18:00, the stress reaches 2.3 MPa, 2.8 MPa and 2.7 MPa, respectively, and the local stress is relatively large, which conforms to the characteristics of short-term rapid change.

As can be seen from Figure 15, under the action of negative temperature difference on the tower wall, the area of tensile stress is mainly concentrated on the outer tower wall. The maximum value is located in the upper part of the western outer tower wall, and the range of tensile stress is mainly diffused along the center of the tower wall to both sides. The reason could be attributed to the principle of heat expansion and cold contraction: the temperature of the inner wall is less changed while the temperature of the outer wall decreases rapidly due to the heat conductivity and lack of solar radiation, which leads to the compressive stress in the inner wall and tensile stress in the outer wall (see Figure 15). The stress at 3:00 and 7:00 reaches 0.1 MPa and 1.3 MPa, respectively. The effect of local stress is less than that of positive temperature difference, and it also conforms to the characteristics of short-term rapid change.

After calculation, the temperature difference stress generated on the outer and inner walls of the 12th section tower column meets the standard value of 2.85 MPa for the tensile strength of C60 concrete specified in the Chinese national standard “Code for Design of Concrete Structures” (GB 50010-2010) [24]. Therefore, in the actual construction and maintenance process of a similar main tower in the future, we should mainly consider the negative effects of positive temperature differences in the day.

## 7. Conclusions

Based on the Nanjing Xinchengwei Yangtze River Bridge, this paper investigates the variation law of temperature field and thermal stress of the main tower. The following conclusions can be drawn.

1. In the daytime, the temperature of the outer wall of the main tower is greater than that of the inner wall, forming a positive temperature difference. During the night, the atmospheric temperature drops rapidly. After the heat transfer effect of concrete from outside to inside for a long time during the day, the temperature of the inner wall is gradually higher than that of the outer wall, forming a negative temperature difference.
2. Under the action of positive temperature difference, the distributing area of tensile stress is mainly concentrated in the inner tower wall. The maximum value is at the corner of the intersection of the tower wall, and the range of tensile stress is mainly diffused along the vertical wall.
3. Under the action of negative temperature difference, the distributing area of tensile stress is mainly concentrated in the outer tower wall. The maximum value is located in the upper part of the western outer tower wall, and the range of tensile stress is mainly diffused along the center of the tower wall to both sides.
4. The maximum tensile stresses in the inner and outer tower walls are 2.8 MPa and 1.3 MPa, respectively, which meets the standard value of 2.85 MPa for the tensile strength of C60 concrete specified in the Chinese national standard.

**Author Contributions:** Conceptualization, M.D.; methodology, M.D.; software, J.Z.; validation, Z.G.; investigation, M.D., J.Z., Z.G. and Z.F.; writing—original draft, M.D. and J.Z.; writing—review and editing, J.X.; supervision, M.D. All authors have read and agreed to the published version of the manuscript.

**Funding:** This research received no external funding.

**Institutional Review Board Statement:** Not applicable.

**Informed Consent Statement:** Informed consent was obtained from all subjects involved in this study.

**Data Availability Statement:** The data that support the findings of this study are available from the corresponding author upon reasonable request.

**Conflicts of Interest:** The authors declare that there are no conflict of interest regarding the publication of this paper.

## References

- Wei, Y.; Xu, P.F.; Zhang, Y.R.; Wang, G.F.; Zheng, K.Q. Compressive behaviour of FRP-steel wire mesh composite tubes filled with seawater and sea sand concrete. *Constr. Build. Mater.* **2021**, *314*, 125608. [\[CrossRef\]](#)
- Yan, Y.H.; Wu, D.J.; Li, Q. A three-dimensional method for the simulation of temperature fields induced by solar radiation. *Adv. Struct. Eng.* **2019**, *22*, 567–580. [\[CrossRef\]](#)
- Liu, W.C.; Cao, W.L.; Yan, H.Q.; Ye, T.X.; Jia, W. Experimental and numerical studies of controlling thermal cracks in mass concrete foundation by circulating water. *Appl. Sci.* **2016**, *6*, 110. [\[CrossRef\]](#)
- Wang, Q.D.; Fu, Z.Q.; Wei, Y.; Wang, Y.X.; Yao, Y. Predicting the ENS-based SCFs of rib-deck welds by integrating HSS measurement. *J. Constr. Steel Res.* **2023**, *203*, 107828.
- Wang, Q.D.; Fu, Z.Q.; Wei, Y.; Wang, Y.X. Fatigue evaluation of the rib-deck weld in OSDs considering the effect of asphalt-steel interface bonding property. *Adv. Struct. Eng.* **2023**, *26*, 1486–1497. [\[CrossRef\]](#)
- Wang, D.; Deng, Y.; Liu, Y.M.; Liu, Y. Numerical investigation of temperature gradient-induced thermal stress for steel–concrete composite bridge deck in suspension bridges. *J. Cent. South Univ.* **2018**, *25*, 185–195. [\[CrossRef\]](#)
- Zhu, C.M.; Wang, Y.Z.; Yan, B.; Gao, H.W. Numerical simulation on real-time temperature field and strength field of bridge mass concrete. *Appl. Mech. Mater.* **2011**, *99–100*, 346–349. [\[CrossRef\]](#)
- Li, Y.; He, S.; Liu, P. Effect of solar temperature field on a sea-crossing cable-stayed bridge tower. *Adv. Struct. Eng.* **2019**, *22*, 1867–1877. [\[CrossRef\]](#)
- Wang, G.Z.; Li, Y.M. Temperature effect analysis of the twin towers concrete cable-stayed bridge for construction control. *Adv. Mater. Res.* **2013**, *671–674*, 1055–1063. [\[CrossRef\]](#)
- Feng, Z.R.; Shen, J.; Wang, X.J. Finite element analysis of thermal stress for cable stayed bridge tower with cracks. *Appl. Mech. Mater.* **2012**, *178–181*, 2085–2090. [\[CrossRef\]](#)
- Huang, Y.H.; Liu, G.X.; Huang, S.P.; Rao, R.; Hu, C.F. Experimental and finite element investigations on the temperature field of a massive bridge pier caused by the hydration heat of concrete. *Constr. Build. Mater.* **2018**, *192*, 240–252. [\[CrossRef\]](#)
- Jin, D.; Liu, X.L.; Wang, B.; Huang, Q. Main girder deflection variations in cable-stayed bridge with temperature over various time scales. *Math. Probl. Eng.* **2020**, *2020*, 4316921. [\[CrossRef\]](#)
- Zhang, Y.H. Research on the Most Unfavorable Temperature Field and Temperature Stress of Long-Span Concrete Box Girder Bridge under Sunlight. Master's Thesis, Southwest Jiaotong University, Chengdu, China, 2017. (In Chinese)
- Fan, J.S.; Liu, Y.F.; Liu, C. Experiment study and refined modeling of temperature field of steel-concrete composite beam bridges. *Eng. Struct.* **2021**, *240*, 112350. [\[CrossRef\]](#)
- Lv, S.S.; Zhu, L.M.; Xing, S.L.; Wang, C.L. Study on sunshine temperature field of concrete box girder based on meteorological parameters. In Proceedings of the International Conference on Advances in Civil Engineering, Energy Resources and Environment Engineering (ACCESSE), Changchun, China, 28–30 June 2019.
- Yang, S.; Li, W.Q.; Huang, X.; Ouyang, X.; Zhu, J.; Li, Y.L. Research on temperature field of steel box girder based on convective heat transfer coefficient correction. *J. South China Univ. Technol. (Nat. Sci. Ed.)* **2021**, *49*, 47–58. (In Chinese)
- Ye, W. Research on Sunshine Temperature Field and Temperature Stress of Railway Prestressed Concrete Box Girder. Master's Thesis, Southwest Jiaotong University, Chengdu, China, 2014. (In Chinese)
- Zhou, H.; Yi, Y.L.; Ye, Z.T.; Li, M. Analysis on temperature field and temperature effect of long-span combined beam cable-stayed bridge. *Bridge Constr.* **2018**, *50*, 50–55. (In Chinese)
- Dai, G.L.; Zhang, Q.Q.; Ge, H.; Rao, H.M. Research on temperature field of concrete box girder based on integral transformation method. *J. Huazhong Univ. Sci. Technol. (Nat. Sci. Ed.)* **2021**, *49*, 77–82.
- Zhang, L.L.; Yang, L.; Yang, T.S.; Zhao, Y.Q.; Liu, H. Temperature field analysis of long-span concrete box girder. *Soil-Wood Build. Environ. Eng.* **2011**, *33*, 36–42.

21. Larsson, O.; Thelandersson, S. Estimating extreme values of thermal gradients in concrete structures. *Mater. Struct.* **2011**, *44*, 1491–1500. [[CrossRef](#)]
22. Ren, X.; Tong, Y.; He, Q.; Huang, P.M. Thermal stress fields of thin-walled box girder concrete bridge tower. *J. Guangxi Univ. Nat. Sci. Ed.* **2011**, *36*, 121–127.
23. Song, Z.W.; Xiao, J.Z.; Shen, L.M. On temperature gradients in high performance concrete box girder under solar radiation. *Adv. Struct. Eng.* **2012**, *15*, 399–415. [[CrossRef](#)]
24. GB 50010-2010; Code for Design Concrete Structures. China Architecture & Building Press: Beijing, China, 2010. (In Chinese)

**Disclaimer/Publisher’s Note:** The statements, opinions and data contained in all publications are solely those of the individual author(s) and contributor(s) and not of MDPI and/or the editor(s). MDPI and/or the editor(s) disclaim responsibility for any injury to people or property resulting from any ideas, methods, instructions or products referred to in the content.